

Constraints imply limited future weakening of Atlantic meridional overturning circulation

David Bonan

dbonan@caltech.edu

California Institute of Technology <https://orcid.org/0000-0003-3867-6009>

Andrew Thompson

California Institute of Technology <https://orcid.org/0000-0003-0322-4811>

Tapio Schneider

California Institute of Technology <https://orcid.org/0000-0001-5687-2287>

Laure Zanna

New York University

Kyle Armour

University of Washington <https://orcid.org/0000-0002-6833-5179>

Shantong Sun

Laoshan Laboratory

Article

Keywords:

Posted Date: June 10th, 2024

DOI: <https://doi.org/10.21203/rs.3.rs-4456168/v1>

License:   This work is licensed under a Creative Commons Attribution 4.0 International License.

[Read Full License](#)

Additional Declarations: There is **NO** Competing Interest.

Version of Record: A version of this preprint was published at Nature Geoscience on May 29th, 2025. See the published version at <https://doi.org/10.1038/s41561-025-01709-0>.

Constraints imply limited future weakening of Atlantic meridional overturning circulation

David B. Bonan¹, Andrew F. Thompson¹, Tapio Schneider¹, Laure Zanna², Kyle C. Armour^{3,4}, Shantong Sun⁵

¹*Environmental Science and Engineering, California Institute of Technology, Pasadena, California, USA*

²*Courant Institute of Mathematical Sciences, New York University, New York City, New York, USA*

³*Department of Atmospheric Sciences, University of Washington, Seattle, Washington, USA*

⁴*School of Oceanography, University of Washington, Seattle, Washington, USA*

⁵*Laoshan Laboratory, Qingdao, China*

Climate models simulate a large spread in the projected weakening of the Atlantic meridional overturning circulation (AMOC) over the 21st century. Here, we demonstrate that this uncertainty can be substantially reduced by using a thermal-wind expression that relates the AMOC strength to the meridional density difference and the overturning depth in the Atlantic basin. This expression captures the intermodel spread in AMOC weakening across climate models, with the majority of the intermodel spread arising from overturning depth changes. The overturning depth also establishes a crucial link between the present-day and future AMOC strength. Climate models with a deeper present-day overturning tend to predict greater shoaling under warming. This occurs because their present-day North Atlantic is less stratified, allowing for a deeper penetration of surface buoyancy flux changes, greater density changes at depth, and, consequently, greater AMOC weakening. By integrating observational constraints, we conclude that, regardless of the emission scenario, the AMOC will only experience modest weakening of about 4 Sv by the end of this century. These results indicate that the uncertainty in 21st-century AMOC weakening, and a propensity to predict strong AMOC weakening, can be primarily attributed to climate model biases in accurately simulating the present-day ocean stratification.

24 State-of-the-art global climate models (GCMs) consistently predict that the Atlantic meridional overturn-
25 ing circulation (AMOC) will weaken in response to rising greenhouse gas concentrations over the 21st
26 century¹⁻⁴. This weakening is important because the AMOC plays a crucial role in ventilating the up-
27 per 2000 m of the ocean⁵ and transporting heat northward throughout the Atlantic Ocean⁶. These pro-
28 cesses regulate Atlantic sea-surface temperatures, which in turn have wide-ranging impacts on regional
29 climates over North America and Western Europe^{7,8}, Arctic sea-ice variability^{9,10}, and the location of tropi-
30 cal precipitation¹¹⁻¹³. Moreover, changes in the AMOC strength are expected to strongly influence regional
31 sea level rise¹⁴⁻¹⁶ and regional climate change¹⁷⁻¹⁹ over the 21st century.

32 While GCMs consistently predict 21st-century AMOC weakening, there is significant intermodel spread in
33 the rate and magnitude of this weakening, adding considerable uncertainty to future climate projections.
34 For instance, GCMs participating in Phase 6 of the Coupled Model Intercomparison Project (CMIP6)²⁰ on
35 average predict that, by the end of the century, the AMOC will weaken by about 8 Sv ($1 \text{ Sv} \equiv 10^6 \text{ m}^3 \text{ s}^{-1}$;
36 black line, Fig. 1). However, some GCMs predict that the AMOC will weaken by as little as 2 Sv, while
37 others predict that it will weaken by as much as 15 Sv (Fig. 1). Interestingly, the magnitude of AMOC
38 weakening depends more on the individual GCM considered than on the emission scenario (Fig. 1).

39 How does the intermodel spread in AMOC projections arise? Over the past few decades, a series of studies
40 have identified a strong correlation between the present-day AMOC strength and AMOC weakening under
41 warming^{4,21-26}. In particular, GCMs with a stronger present-day AMOC exhibit greater AMOC weaken-
42 ing. Indeed, the CMIP6 GCMs with the strongest present-day (1981–2010) AMOC tend to exhibit the most
43 AMOC weakening, predicting a decrease of 10–15 Sv by the end of the 21st century (red lines and bars,
44 Fig. 1d). Similarly, the CMIP6 GCMs with the weakest present-day AMOC tend to exhibit the least AMOC
45 weakening, predicting a decrease of 3–6 Sv by the end of the 21st century (blue lines and bars, Fig. 1d).

46 This implies that the observed AMOC strength can be used to estimate the magnitude of AMOC weakening
47 expected in the 21st century via a so-called ‘emergent constraint,’ which describes a statistical relation-
48 ship between aspects of the present-day climate and future changes across GCMs. When combined with
49 observations, emergent constraints can be used to reduce uncertainty in future climate projections.

50 Leveraging any emergent constraint to reduce uncertainty in future climate projections, however, requires a
51 solid understanding of the underlying mechanisms on which the constraint depends²⁷. In this case, the mech-
52 anisms underpinning the correlation between the present-day AMOC strength and future AMOC weakening
53 remain unclear. It has been suggested that the present-day AMOC relates to AMOC weakening under warm-
54 ing through subsurface stratification in the Labrador Sea, as GCMs with weaker present-day Labrador Sea
55 stratification tend to show greater AMOC weakening²⁶. Yet, this explanation for AMOC weakening remains
56 unclear as the Labrador Sea makes a limited contribution to dense water formation in most GCMs²⁸. A bet-
57 ter understanding of the relationship between the present-day AMOC and its projected changes is necessary
58 to constrain 21st-century AMOC projections.

59 Here, we present a physical mechanism that explains the relationship between the present-day and future
60 AMOC strength. The mechanism is rooted in thermal-wind balance, which relates the AMOC strength to the
61 meridional density difference and overturning depth in the Atlantic basin. We show that the primary source
62 of intermodel spread in AMOC weakening arises from changes in the overturning depth. The overturning
63 depth also links the present-day and future AMOC strength. In GCMs with a deeper present-day overturning,
64 the AMOC tends to shoal more under warming because the present-day North Atlantic is less stratified. This
65 allows for greater density changes at depth, which leads to greater AMOC weakening. We use this relation
66 and observations to constrain future AMOC projections and demonstrate that, irrespective of the emission
67 scenario, the AMOC will likely experience only modest weakening over the 21st century.

68 **Controls on Atlantic meridional overturning circulation weakening**

69 The depth-varying transport of the Atlantic basin overturning circulation can be related to the vertical struc-
 70 ture of the meridional density gradient through thermal-wind balance²⁹, which has been shown to provide a
 71 good approximation of the AMOC strength in comprehensive GCMs³⁰⁻³⁴. The vertical structure of the den-
 72 sity gradient can be decomposed into two factors, representing a characteristic magnitude of the meridional
 73 density difference between the high- and low-latitude Atlantic $\Delta_y\rho$ and a characteristic overturning depth
 74 H (see Methods). The AMOC strength ψ from thermal-wind balance can then be expressed as

$$\psi = \frac{g}{2\rho_0 f_0} (\Delta_y\rho) H^2, \quad (1)$$

75 where $g = 9.81 \text{ m s}^{-2}$ is the gravitational acceleration, $\rho_0 = 1027.5 \text{ kg m}^{-3}$ is a reference density of
 76 seawater, and $f_0 = 10^{-4} \text{ s}^{-1}$ is the Coriolis parameter near 40°N. The two key factors, $\Delta_y\rho$ and H , can be
 77 diagnosed directly from CMIP6 output (see Methods). Eq. (1) has previously been shown to provide a good
 78 approximation of the present-day AMOC strength in GCMs³⁴. By linearizing Eq. (1), the change in AMOC
 79 strength $\delta\psi$ can be decomposed as

$$\delta\psi = \frac{g}{2\rho_0 f_0} \left(\underbrace{H^2 \delta(\Delta_y\rho)}_{(A)} + \underbrace{2(\Delta_y\rho) H \delta H}_{(B)} + \underbrace{\epsilon}_{(C)} \right), \quad (2)$$

80 where (A) represents the AMOC strength change due to a change in $\Delta_y\rho$; (B) represents the AMOC strength
 81 change due to a change in H ; and (C) represents the residual AMOC strength change due to higher-order
 82 terms.

83 The thermal-wind expression (Eq. 2) captures the AMOC weakening simulated by CMIP6 GCMs at the
 84 end of the 21st century. It accounts for approximately 75% of the intermodel variance in AMOC strength
 85 changes and exhibits a root-mean-square error of approximately 1 Sv for each emission scenario (Fig. 2a-c).

86 Furthermore, GCMs that simulate small or large AMOC weakening tend to exhibit small or large AMOC
87 weakening based on thermal-wind balance (Fig. 2).

88 The ability of the thermal-wind expression to emulate the AMOC weakening in GCMs implies that H
89 and $\Delta_y\rho$ can explain why the present-day AMOC is related to the magnitude of AMOC weakening under
90 warming. Both Term A and Term B can link the present-day AMOC to future AMOC weakening due to
91 their dependence on present-day H and $\Delta_y\rho$ (see Eq. 2). Term B, which represents the AMOC strength
92 change due to δH , is responsible for the majority of the intermodel spread in AMOC weakening, accounting
93 for 74%, 63%, and 61% of the intermodel variance for the SSP1-2.6, SSP2-4.5, and SSP5-8.5 emission
94 scenarios, respectively (hatched bars, Fig. 2a-c). Term B also shows that GCMs with a greater present-day
95 AMOC exhibit greater AMOC weakening. Term A, which represents the AMOC strength change due to
96 $\delta(\Delta_y\rho)$, accounts for a smaller fraction of intermodel variance: 33%, 25%, and 16% for the SSP1-2.6,
97 SSP2-4.5, and SSP5-8.5 emission scenarios, respectively (open bars, Fig. 2a-c). Term A contributes little to
98 the relationship between the present-day and future AMOC strength.

99 Term B in each individual GCM is similar across the different emission scenarios, indicating that the reason
100 the AMOC weakens similarly across different emission scenarios is due to δH (hatched bars, Fig. 2a-c).
101 Changes in $\Delta_y\rho$ are indeed greater in SSP5-8.5 than in SSP1-2.6, but overall $\delta(\Delta_y\rho)$ does not contribute
102 much to the intermodel spread (open bars, Fig. 2a-c). Given that GCMs with a stronger present-day AMOC
103 tend to exhibit a greater H^{34} , these results indicate that GCMs with a greater H also have a greater δH
104 under warming.

105 To understand the processes contributing to δH and its relationship to H , we examine changes to the vertical
106 structure of the Atlantic basin density difference $\Delta_y\rho(z)$, which determines the magnitude of δH (see

107 Methods). For example, because H depends on the vertically-integrated $\Delta_y\rho(z)$, a small reduction in $\Delta_y\rho$
108 throughout the water column would lead to more shoaling of H . Conversely, a large reduction in $\Delta_y\rho$ that is
109 confined to the surface ocean would lead to less shoaling of H . Scaling arguments also suggest that H can
110 be linked to the stratification (N^2) of the North Atlantic³⁴. A strong present-day North Atlantic N^2 would
111 limit δH by inhibiting the vertical penetration of surface buoyancy flux anomalies that can alter Atlantic
112 basin density. Indeed, we find that GCMs with a weaker present-day AMOC exhibit stronger present-day
113 N^2 in the North Atlantic (40°N–65°N, 50–1000 m; Fig. 3a). The impact of present-day North Atlantic
114 N^2 on $\Delta_y\rho(z)$ change can be seen in vertical profiles of North Atlantic (40°N–65°N) density change,
115 which contributes more to $\Delta_y\rho(z)$ changes when compared to low-latitude (30°S–30°N) Atlantic density
116 changes. Grouping together GCMs with a strong present-day AMOC (red) and a weak present-day AMOC
117 (blue) shows that a strong present-day AMOC and weak present-day North Atlantic N^2 correspond to more
118 vertically uniform North Atlantic density changes. In particular, density changes between 1000 and 2000 m
119 are similar to density changes between 0 and 200 m, consistent with deeper mixing of surface buoyancy flux
120 anomalies (red lines, Fig. 3b-d). Conversely, GCMs with a weak present-day AMOC and strong present-
121 day North Atlantic N^2 tend to exhibit weaker North Atlantic density changes at depth and stronger density
122 changes at the surface, indicating shallower mixing of surface buoyancy flux anomalies (blue lines, Fig.
123 3b-d).

124 The results above demonstrate that the present-day North Atlantic N^2 strongly controls vertical density
125 changes in the North Atlantic, which determines the magnitude of AMOC weakening through δH . These
126 results can be summarized by a schematic that depicts GCMs with a weak present-day AMOC (Fig. 4a)
127 and a strong present-day AMOC (Fig. 4b). In GCMs with a weak present-day AMOC, the AMOC tends to
128 be shallow (smaller H) and the North Atlantic tends to be strongly stratified (greater N^2). Under warming,

129 any change to ocean density from surface buoyancy flux anomalies will occur closer to the surface and will
130 not penetrate deeply into the interior of the North Atlantic, leading to weaker density changes at depth. This
131 results in smaller δH and thus smaller AMOC weakening. Conversely, in GCMs with a strong present-day
132 AMOC, the AMOC tends to be deeper (greater H) and the North Atlantic tends to be weakly stratified
133 (smaller N^2). Under warming, the same surface buoyancy flux anomalies will penetrate more deeply into
134 the interior of the North Atlantic, leading to stronger density changes at depth. This results in greater δH
135 and thus greater AMOC weakening.

136 **Constraining Atlantic meridional overturning circulation weakening**

137 We can now leverage this mechanistic understanding of AMOC weakening to constrain AMOC projections
138 over the 21st century (see Methods). The unconstrained probability density function (PDF) of CMIP6
139 projections suggest that, regardless of the emission scenario, the AMOC most likely will weaken by about
140 8 Sv at the end of the 21st century (black PDFs, Fig. 5). However, there is considerable intermodel spread,
141 with a high likelihood of even greater AMOC weakening (~ 15 Sv).

142 The previously identified relationship between the present-day and future AMOC strength can be used
143 to constrain AMOC projections by using present-day observations. The AMOC strength diagnosed from
144 the observationally-constrained ECCO state estimate³⁵ and the linear regression of the present-day AMOC
145 against the future AMOC change (see Methods) suggests that the AMOC will only weaken by about 4 Sv at
146 the end of the 21st century (blue PDFs, Fig. 5). The likelihood of a strong AMOC weakening is substantially
147 reduced, with an AMOC decline greater than 9 Sv being extremely unlikely for all emission scenarios (blue
148 PDFs, Fig. 5).

149 Can we trust the linear relationship between the present-day and future AMOC strength? Considering that
 150 thermal-wind balance accounts for a large portion of the intermodel variance in AMOC weakening, we can
 151 examine this assumption by constructing a simple physical expression that links the present-day and future
 152 AMOC strength. The AMOC strength change $\delta\psi$ based on thermal-wind can be mainly attributed to δH
 153 (Term B in Eq. 2), resulting in

$$\delta\psi \approx \frac{g}{\rho_0 f_0} \overline{(\Delta_y \rho)} H \delta H, \quad (3)$$

154 where the overline indicates the multi-model mean value of $\Delta_y \rho$, which contributes relatively little to the
 155 intermodel spread of the present-day AMOC³⁴. Because δH depends on H and $\overline{(\Delta_y \rho)}$ is a constant, the above
 156 expression can be related solely to the present-day AMOC strength ψ via regression analysis of H and δH ,
 157 which results in

$$\delta\psi \approx \frac{g}{\rho_0 f_0} \overline{(\Delta_y \rho)} H(\psi) [\alpha_H + \beta_H H(\psi)], \quad (4)$$

158 where a_H is the intercept and b_H is the slope of the linear regression of δH on H . Furthermore, because we
 159 have assumed that $\Delta_y \rho$ is a constant, ψ is a function of H only (Eq. 1), enabling us to invert H and make it
 160 a function of ψ , which results in

$$H(\psi) = \sqrt{\frac{2\rho_0 f_0 \psi}{g(\Delta_y \rho)}}. \quad (5)$$

161 Eq. (4) predicts $\delta\psi$ solely from ψ via H and thus provides a physical understanding of the statistical
 162 relationship between the present-day and future AMOC strength in GCMs.

163 The physical expression (Eq. 4) describes the AMOC weakening in GCMs slightly more accurately than
 164 the linear regression of future AMOC change based on the present-day AMOC strength (compare orange
 165 and blue lines, Fig. 5). Eq. (4) better captures the greater AMOC weakening simulated by GCMs with a
 166 stronger present-day AMOC because $\delta\psi$ depends non-linearly on H . Using the PDF of observed AMOC
 167 strength from ECCO with the prediction of $\delta\psi$ from Eq. (4) (see Methods) gives a further refined estimate

168 of future AMOC weakening (orange PDFs, Fig. 5). The constrained estimate also suggests that the AMOC
169 will weaken by about 4 Sv by 2071–2100 under all emission scenarios. Importantly, for SSP5-8.5, greater
170 AMOC weakening is even less likely with this constraint than based on the linear relationship (compare blue
171 and orange PDFs, Fig. 5c).

172 These results show that because GCMs simulate a stronger present-day AMOC relative to observations,
173 GCMs also simulate excessive AMOC weakening over the 21st century. This emergent constraint, which
174 we predict from a simple physical expression, corrects these biases and implies that we can expect modest
175 AMOC weakening over the 21st century.

176 **Implications for 21st-century climate projections**

177 In recent years, several studies have raised concerns about a potential collapse of the AMOC in the 21st
178 century^{36–38}. These studies argue that independent proxies for the AMOC strength indicate either bi-stable
179 AMOC states or early warnings of AMOC instability in the present climate. However, it has also been argued
180 that some of these studies, particularly those employing statistical models³⁷, may produce false alarms of
181 AMOC collapse due to artificial increases in variance³⁹. While our study does not directly investigate
182 indicators of AMOC collapse, our findings suggest an AMOC collapse during the 21st century is unlikely.
183 In fact, our approach, which uses a physically based relation instead of a statistical model, suggests that
184 AMOC weakening over the 21st century, as simulated by contemporary GCMs, will be modest.

185 One reason why our conclusions imply modest AMOC weakening could be that contemporary GCMs suf-
186 fer from a freshwater transport bias that favors a stable AMOC in the present-day climate^{36,40,41}. This
187 model bias also affects the stratification of the Atlantic basin and thus H . Ref. 36 corrected this freshwater

188 transport bias in a comprehensive GCM and showed that the AMOC would eventually collapse, although
189 this occurred a few centuries after the abrupt forcing, suggesting no imminent collapse in the 21st century.
190 Furthermore, it has been argued that the freshwater transport criteria does not accurately describe ocean
191 circulation behavior in GCMs⁴², casting doubt on the usefulness of freshwater transport as an indicator of
192 a possible AMOC collapse. While recent work has found evidence of AMOC bi-stability in comprehen-
193 sive GCMs⁴³⁻⁴⁵, these results depend on large freshwater forcing, which is not expected to occur during
194 the 21st century. Additionally, 21st-century AMOC weakening has been mainly attributed to surface heat
195 flux changes^{21,46}, calling into question the usefulness of examining the potential for a 21st-century AMOC
196 collapse through freshwater hosing experiments.

197 The key takeaway of this work is that a physically based constraint implies the AMOC will undergo modest
198 weakening over the 21st century. This constraint is relatively independent of the magnitude of greenhouse
199 gas forcing, and explains why AMOC projections over the 21st century are similar for GCMs across different
200 emission scenarios: the present-day Atlantic basin stratification largely determines the degree of AMOC
201 weakening in the 21st century. This indicates that uncertainty in 21st-century AMOC projections is primarily
202 related to intermodel differences in the present-day ocean state rather than the emission scenario. This study
203 adds to a growing body of work that indicates the behavior of the ocean under transient climate change is
204 closely tied to the background ocean state^{25,47,48}. Therefore, improving the representation of processes that
205 determine the present-day ocean state will also likely improve future climate projections.

206 **Methods**

207 **CMIP6 output** This analysis includes all CMIP6 models²⁰ from the r1i1p1f1 variant label that provide
208 monthly output of ocean potential temperature (thetao), ocean absolute salinity (so), and the meridional

209 overturning streamfunction (msftmz or msftmy) for historical, SSP1-2.6, SSP2-4.5, and SSP5-8.5 emission
 210 scenarios. Model names are provided in Figures 1–3. The present-day climatological time period is 1981–
 211 2010, and the SSP climatological time period is 2071–2100. The AMOC strength is defined as the maximum
 212 value of the meridional overturning streamfunction in the Atlantic basin northward of 30°S and below 500 m.
 213 The choice of 500 m avoids volume flux contributions associated with the subtropical ocean gyres. Ocean
 214 potential density is calculated from ocean potential temperature and ocean absolute salinity and referenced to
 215 2000 dbar using the Gibbs SeaWater Oceanographic Toolbox of TEOS-10⁴⁹. The Brunt-Väisälä frequency
 216 N^2 is calculated from ocean potential density ρ as

$$N^2 = -\frac{g}{\rho_0} \frac{\partial \rho}{\partial z}, \quad (6)$$

217 and used to indicate stratification of the North Atlantic (40°N–65°N, 50–1000 m).

218 **Observations** Observational estimates of the AMOC strength are obtained from the ECCOV4r3 (ECCO)
 219 state estimate³⁵. ECCO is based on the MITgcm ocean model⁵⁰ at 1° resolution with 50 vertical levels.
 220 The state estimate is iteratively improved by modifying ocean model initial conditions, parameters, and
 221 atmospheric boundary conditions to minimize model-observation disagreement. ECCO output is used to
 222 calculate the maximum value of the meridional overturning streamfunction in the Atlantic basin, which is
 223 consistent with the definition of the AMOC strength in CMIP6 models. The observed AMOC strength can
 224 also be estimated from the Rapid Meridional Overturning Circulation (RAPID) mooring array⁵¹, which was
 225 deployed in 2004 to continuously monitor the meridional overturning circulation in the Atlantic basin at
 226 26.5°N. However, this estimate of the AMOC strength is inconsistent with our definition of the AMOC
 227 strength from CMIP6 GCMs. A previous study showed that the AMOC strength from ECCO at 26.5°N
 228 is in good agreement with the RAPID array⁵², which indicates that ECCO provides a suitable estimate of
 229 the observed AMOC strength. The annual-mean AMOC strength from ECCO is calculated over the period

230 1992–2015 and has a mean and standard deviation of 15.3 Sv and 1.2 Sv, respectively.

231 **Thermal-wind expression** The thermal-wind expression (Eq. 1) approximates the AMOC strength as a
 232 function of the Atlantic basin meridional density difference ($\Delta_y\rho$) and overturning depth (H) under an
 233 assumption of mass conservation between zonal and meridional volume transport²⁹. The two terms, $\Delta_y\rho$
 234 and H , are diagnosed from CMIP6 output. Building on efforts by Ref. 30 and Ref. 34, we estimate $\Delta_y\rho$ and
 235 H from the ocean potential density in the Atlantic basin. The term $\Delta_y\rho$ is calculated as the vertical average
 236 of the difference in potential density between the North Atlantic (area-averaged from 40°N to 65°N) and
 237 the low-latitude Atlantic (area-averaged from 30°S to 30°N) over the upper 2000 m of the Atlantic basin.
 238 This estimate of $\Delta_y\rho$ represents the magnitude of the meridional density gradient in the upper cell. The
 239 depth H is calculated as the depth where the depth-integrated $\Delta_y\rho$ (for the same regional domains) equals
 240 the vertical mean of the depth-integrated $\Delta_y\rho$. This estimate of H is approximately the depth of maximum
 241 zonal volume transport³⁰, and assuming weak eastern boundary currents, can be thought of as the depth of
 242 maximum meridional volume transport.

243 **Emergent constraint analysis** To obtain a constrained PDF of the change in the AMOC strength $\delta\psi$ for the
 244 years 2071–2100, we first calculate a PDF of the observed AMOC strength ψ using ECCO (see subsection
 245 above). We assume the PDF of ψ is Gaussian,

$$P(\psi) = \frac{1}{\sqrt{2\pi\sigma_\psi^2}} \exp\left\{-\frac{(\psi - \bar{\psi})^2}{2\sigma_\psi^2}\right\}, \quad (7)$$

246 where $\bar{\psi}$ is the mean and σ_ψ is the standard deviation of the observed AMOC strength. We then create a
 247 constrained PDF of $\delta\psi$ by combining the PDF of the observed AMOC strength $P(\psi)$ and the PDF of the
 248 emergent constraint relationship, which estimates $\delta\psi$ given ψ . The emergent constraint PDF is

$$P\{\delta\psi|\psi\} = \frac{1}{\sqrt{2\pi\sigma_f^2}} \exp\left\{-\frac{(\delta\psi - f(\psi))^2}{2\sigma_f^2}\right\}, \quad (8)$$

249 where σ_f is the prediction error of the regression and $f(\psi)$ estimates $\delta\psi$ based on ψ (which is described in
250 more detail below). Given these two PDFs, $P(\psi)$ and $P\{\delta\psi|\psi\}$, the PDF for $\delta\psi$ is calculated by numerically
251 integrating

$$P(\delta\psi) = \int_{-\infty}^{\infty} P\{\delta\psi|\psi\} P(\psi) d\psi. \quad (9)$$

252 In Eq. (8), $f(\psi)$ is estimated in two separate ways. The first estimate of $f(\psi)$ comes from a linear regression
253 of ψ and $\delta\psi$ based directly on CMIP6 output. This results in

$$f(\psi) = a_\psi + b_\psi\psi, \quad (10)$$

254 where a_ψ is the intercept and b_ψ is the slope of the linear regression of $\delta\psi$ on ψ . The second estimate of
255 $f(\psi)$ comes from the physical expression introduced in this study, which approximates $\delta\psi$ through Eq. (4).

- 257 1. Schmittner, A., Latif, M. & Schneider, B. Model projections of the North Atlantic thermohaline circu-
258 lation for the 21st century assessed by observations. *Geophysical Research Letters* **32** (2005).
- 259 2. Cheng, W., Chiang, J. C. & Zhang, D. Atlantic meridional overturning circulation (AMOC) in CMIP5
260 models: RCP and historical simulations. *Journal of Climate* **26**, 7187–7197 (2013).
- 261 3. Reintges, A., Martin, T., Latif, M. & Keenlyside, N. S. Uncertainty in twenty-first century projections
262 of the Atlantic Meridional Overturning Circulation in CMIP3 and CMIP5 models. *Climate Dynamics*
263 **49**, 1495–1511 (2017).
- 264 4. Weijer, W., Cheng, W., Garuba, O. A., Hu, A. & Nadiga, B. CMIP6 models predict significant 21st
265 century decline of the Atlantic meridional overturning circulation. *Geophysical Research Letters* **47**,
266 e2019GL086075 (2020).
- 267 5. Buckley, M. W. & Marshall, J. Observations, inferences, and mechanisms of the Atlantic Meridional
268 Overturning Circulation: A review. *Reviews of Geophysics* **54**, 5–63 (2016).

- 269 6. Ganachaud, A. & Wunsch, C. Large-scale ocean heat and freshwater transports during the World Ocean
270 Circulation Experiment. *Journal of Climate* **16**, 696–705 (2003).
- 271 7. Zhang, R. & Delworth, T. L. Impact of Atlantic multidecadal oscillations on India/Sahel rainfall and
272 Atlantic hurricanes. *Geophysical research letters* **33** (2006).
- 273 8. Zhang, R. *et al.* A review of the role of the Atlantic meridional overturning circulation in Atlantic
274 multidecadal variability and associated climate impacts. *Reviews of Geophysics* **57**, 316–375 (2019).
- 275 9. Mahajan, S., Zhang, R. & Delworth, T. L. Impact of the Atlantic meridional overturning circulation
276 (AMOC) on Arctic surface air temperature and sea ice variability. *Journal of Climate* **24**, 6573–6581
277 (2011).
- 278 10. Day, J. J., Hargreaves, J., Annan, J. & Abe-Ouchi, A. Sources of multi-decadal variability in Arctic sea
279 ice extent. *Environmental Research Letters* **7**, 034011 (2012).
- 280 11. Frierson, D. M. *et al.* Contribution of ocean overturning circulation to tropical rainfall peak in the
281 Northern Hemisphere. *Nature Geoscience* **6**, 940–944 (2013).
- 282 12. Schneider, T., Bischoff, T. & Haug, G. H. Migrations and dynamics of the intertropical convergence
283 zone. *Nature* **513**, 45–53 (2014).
- 284 13. Marshall, J., Donohoe, A., Ferreira, D. & McGee, D. The ocean’s role in setting the mean position of
285 the Inter-Tropical Convergence Zone. *Climate Dynamics* **42**, 1967–1979 (2014).
- 286 14. Yin, J., Griffies, S. M. & Stouffer, R. J. Spatial variability of sea level rise in twenty-first century
287 projections. *Journal of Climate* **23**, 4585–4607 (2010).

- 288 15. Gregory, J. M. *et al.* The Flux-Anomaly-Forced Model Intercomparison Project (FAFMIP) contribution
289 to CMIP6: Investigation of sea-level and ocean climate change in response to CO₂ forcing. *Geoscientific Model Development* **9**, 3993–4017 (2016).
290
- 291 16. Saenko, O. A., Yang, D. & Myers, P. G. Response of the North Atlantic dynamic sea level and circula-
292 tion to Greenland meltwater and climate change in an eddy-permitting ocean model. *Climate Dynamics*
293 **49**, 2895–2910 (2017).
- 294 17. Vellinga, M. & Wood, R. A. Impacts of thermohaline circulation shutdown in the twenty-first century.
295 *Climatic Change* **91**, 43–63 (2008).
- 296 18. Jackson, L. *et al.* Global and European climate impacts of a slowdown of the AMOC in a high resolution
297 GCM. *Climate dynamics* **45**, 3299–3316 (2015).
- 298 19. Liu, W., Fedorov, A. V., Xie, S.-P. & Hu, S. Climate impacts of a weakened Atlantic Meridional
299 Overturning Circulation in a warming climate. *Science Advances* **6**, eaaz4876 (2020).
- 300 20. Eyring, V. *et al.* Overview of the Coupled Model Intercomparison Project Phase 6 (CMIP6) experimen-
301 tal design and organization. *Geoscientific Model Development* **9**, 1937–1958 (2016).
- 302 21. Gregory, J. *et al.* A model intercomparison of changes in the Atlantic thermohaline circulation in
303 response to increasing atmospheric CO₂ concentration. *Geophysical Research Letters* **32** (2005).
- 304 22. Gregory, J. M. & Tailleux, R. Kinetic energy analysis of the response of the Atlantic meridional over-
305 turning circulation to CO₂-forced climate change. *Climate dynamics* **37**, 893–914 (2011).
- 306 23. Weaver, A. J. *et al.* Stability of the Atlantic meridional overturning circulation: A model intercompari-
307 son. *Geophysical Research Letters* **39** (2012).

- 308 24. Kostov, Y., Armour, K. C. & Marshall, J. Impact of the Atlantic meridional overturning circulation on
309 ocean heat storage and transient climate change. *Geophysical Research Letters* **41**, 2108–2116 (2014).
- 310 25. Winton, M. *et al.* Has coarse ocean resolution biased simulations of transient climate sensitivity? *Geo-*
311 *physical Research Letters* **41**, 8522–8529 (2014).
- 312 26. Lin, Y.-J., Rose, B. E. & Hwang, Y.-T. Mean state AMOC affects AMOC weakening through subsurface
313 warming in the Labrador Sea. *Journal of Climate* **36**, 3895–3915 (2023).
- 314 27. Hall, A., Cox, P., Huntingford, C. & Klein, S. Progressing emergent constraints on future climate
315 change. *Nature Climate Change* **9**, 269–278 (2019).
- 316 28. Jackson, L. & Petit, T. North Atlantic overturning and water mass transformation in CMIP6 models.
317 *Climate Dynamics* **60**, 2871–2891 (2023).
- 318 29. Nikurashin, M. & Vallis, G. A theory of the interhemispheric meridional overturning circulation and
319 associated stratification. *Journal of Physical Oceanography* **42**, 1652–1667 (2012).
- 320 30. De Boer, A. M., Gnanadesikan, A., Edwards, N. R. & Watson, A. J. Meridional density gradients do not
321 control the Atlantic overturning circulation. *Journal of Physical Oceanography* **40**, 368–380 (2010).
- 322 31. Jansen, M. F., Nadeau, L.-P. & Merlis, T. M. Transient versus equilibrium response of the ocean's
323 overturning circulation to warming. *Journal of Climate* **31**, 5147–5163 (2018).
- 324 32. Sigmond, M., Fyfe, J. C., Saenko, O. A. & Swart, N. C. Ongoing AMOC and related sea-level and
325 temperature changes after achieving the Paris targets. *Nature Climate Change* **10**, 672–677 (2020).
- 326 33. Bonan, D. B., Thompson, A. F., Newsom, E. R., Sun, S. & Rugenstein, M. Transient and equilibrium
327 responses of the Atlantic overturning circulation to warming in coupled climate models: The role of
328 temperature and salinity. *Journal of Climate* **35**, 5173–5193 (2022).

- 329 34. Nayak, M. S., Bonan, D. B., Newsom, E. R. & Thompson, A. F. Controls on the strength and structure
330 of the Atlantic meridional overturning circulation in climate models. *Geophysical Research Letters* **51**,
331 e2024GL109055 (2024).
- 332 35. Forget, G. *et al.* ECCO version 4: An integrated framework for non-linear inverse modeling and global
333 ocean state estimation. *Geoscientific Model Development* **8**, 3071–3104 (2015).
- 334 36. Liu, W., Xie, S.-P., Liu, Z. & Zhu, J. Overlooked possibility of a collapsed Atlantic Meridional Over-
335 turning Circulation in warming climate. *Science Advances* **3**, e1601666 (2017).
- 336 37. Boers, N. Observation-based early-warning signals for a collapse of the Atlantic Meridional Overturn-
337 ing Circulation. *Nature Climate Change* **11**, 680–688 (2021).
- 338 38. Ditlevsen, P. & Ditlevsen, S. Warning of a forthcoming collapse of the Atlantic meridional overturning
339 circulation. *Nature Communications* **14**, 1–12 (2023).
- 340 39. Chen, X. & Tung, K.-K. Evidence lacking for a pending collapse of the Atlantic Meridional Overturning
341 Circulation. *Nature Climate Change* **14**, 40–42 (2024).
- 342 40. Hofmann, M. & Rahmstorf, S. On the stability of the Atlantic meridional overturning circulation.
343 *Proceedings of the National Academy of Sciences* **106**, 20584–20589 (2009).
- 344 41. Jackson, L. C. *et al.* Challenges simulating the AMOC in climate models. *Philosophical Transactions*
345 *of the Royal Society A* **381**, 20220187 (2023).
- 346 42. Gent, P. R. A commentary on the Atlantic meridional overturning circulation stability in climate models.
347 *Ocean Modelling* **122**, 57–66 (2018).
- 348 43. Rahmstorf, S. Bifurcations of the Atlantic thermohaline circulation in response to changes in the hy-
349 drological cycle. *Nature* **378**, 145–149 (1995).

- 350 44. Boulton, C. A., Allison, L. C. & Lenton, T. M. Early warning signals of Atlantic Meridional Overturning
351 Circulation collapse in a fully coupled climate model. *Nature communications* **5**, 5752 (2014).
- 352 45. van Westen, R. M., Kliphuis, M. & Dijkstra, H. A. Physics-based early warning signal shows that
353 AMOC is on tipping course. *Science Advances* **10**, eadk1189 (2024).
- 354 46. Maroon, E. A., Kay, J. E. & Karnauskas, K. B. Influence of the Atlantic meridional overturning circula-
355 tion on the Northern Hemisphere surface temperature response to radiative forcing. *Journal of Climate*
356 **31**, 9207–9224 (2018).
- 357 47. He, J., Winton, M., Vecchi, G., Jia, L. & Rugestein, M. Transient climate sensitivity depends on base
358 climate ocean circulation. *Journal of Climate* **30**, 1493–1504 (2017).
- 359 48. Newsom, E., Zanna, L. & Gregory, J. Background pycnocline depth constrains future ocean heat uptake
360 efficiency. *Geophysical Research Letters* **50**, e2023GL105673 (2023).
- 361 49. McDougall, T. J. & Barker, P. M. Getting started with TEOS-10 and the Gibbs Seawater (GSW) oceanog-
362 raphic toolbox. *SCOR/IAPSO WG127* **127**, 1–28 (2011).
- 363 50. Marshall, J., Adcroft, A., Hill, C., Perelman, L. & Heisey, C. A finite-volume, incompressible Navier
364 Stokes model for studies of the ocean on parallel computers. *Journal of Geophysical Research: Oceans*
365 **102**, 5753–5766 (1997).
- 366 51. Cunningham, S. A. *et al.* Temporal variability of the Atlantic meridional overturning circulation at 26.5
367 N. *Science* **317**, 935–938 (2007).
- 368 52. Kostov, Y. *et al.* Distinct sources of interannual subtropical and subpolar Atlantic overturning variabil-
369 ity. *Nature Geoscience* **14**, 491–495 (2021).

370 **Acknowledgements** The authors thank the climate modeling groups for producing and making available their model
371 output, which is accessible at the Earth System Grid Federation (ESGF) Portal (<https://esgf-node.llnl.gov/search/cmip6/>).
372 D.B.B was supported by the National Science Foundation (NSF) Graduate Research Fellowship Program (NSF Grant
373 DGE1745301). A.F.T. was supported by the David and Lucile Packard Foundation and NSF Award OCE-1756956.
374 T.S. was supported by Schmidt Sciences, LLC. L.Z. was supported by Schmidt Sciences, LLC. K.C.A was supported
375 by NSF Awards OCE-1850900 and AGS-1752796 and a Calvin Professorship in Oceanography.

376 **Competing Interests** The authors declare that they have no competing financial interests.

377 **Correspondence** Correspondence and requests for materials should be addressed to David B. Bonan (email: dbo-
378 nan@caltech.edu).

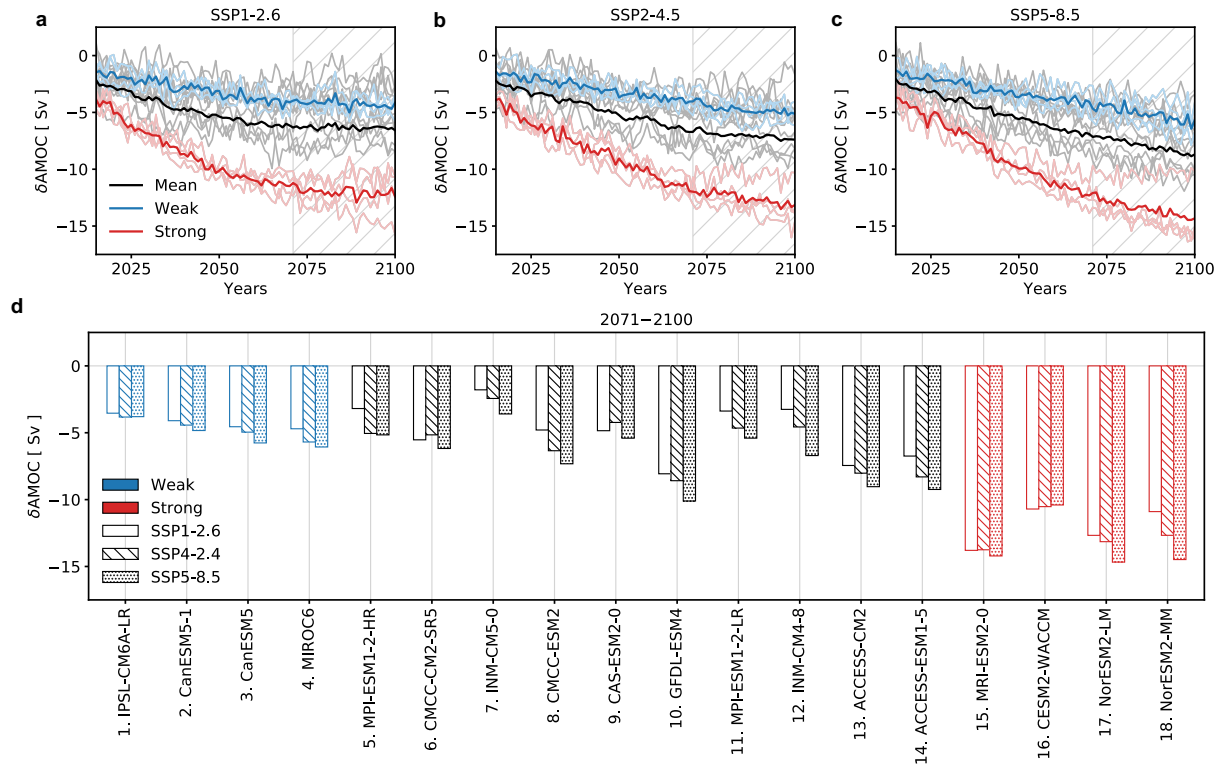


Figure 1: Relationship between the present-day and future AMOC strength. Timeseries of the change in AMOC strength for GCMs participating in CMIP6 under (a) SSP1-2.6, (b) SSP2-4.5, and (c) SSP5-8.5 emission scenarios. The thick lines denote the average of the four GCMs with the strongest present-day AMOC (red), the four GCMs with the weakest present-day AMOC (blue), and all other GCMs (black). Each thin line denotes an individual GCM. (d) The change in AMOC strength for GCMs under SSP1-2.6 (open bar), SSP2-4.5 (hatched bar), and SSP5-8.5 (dotted bar) emission scenarios. The present-day time period is 1981–2010 and the SSP time period is 2071–2100, as indicated by the grey hatches in (a-c). GCMs in (d) are ordered from weak to strong present-day AMOC.

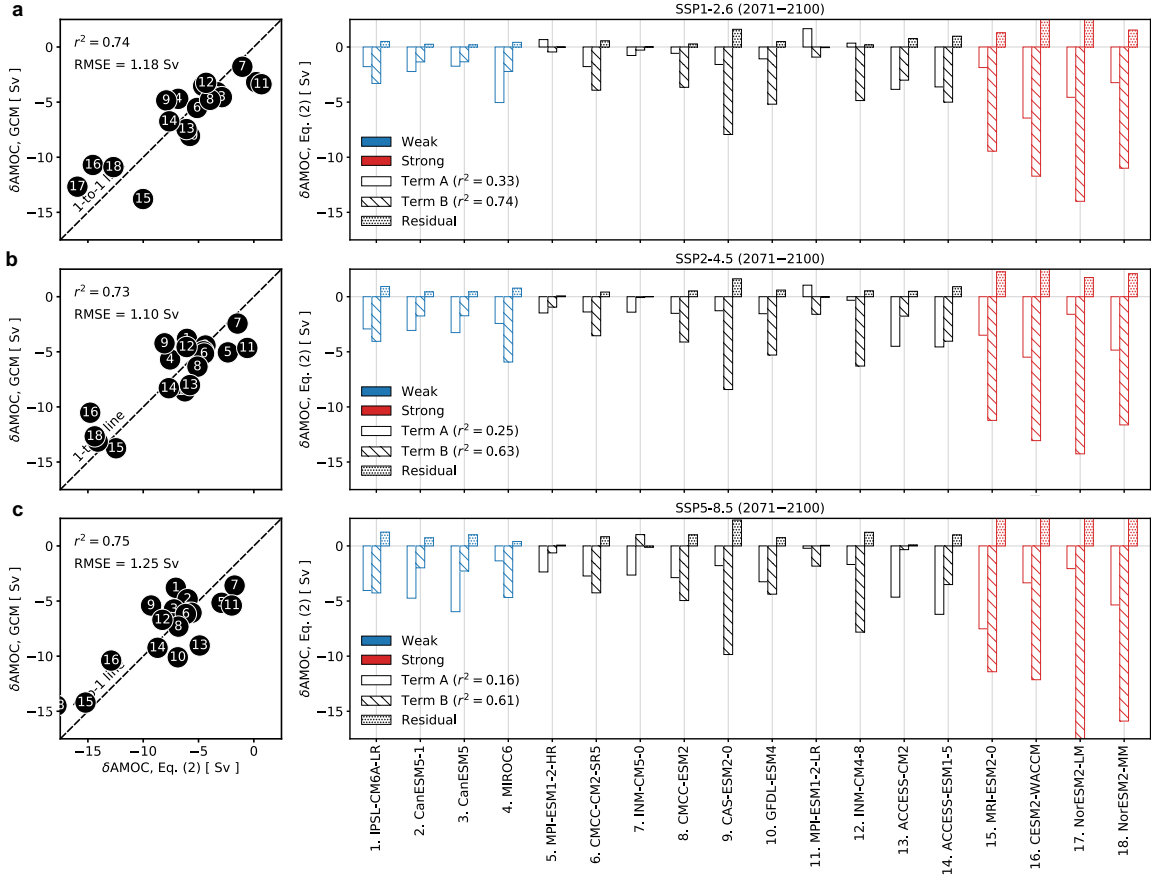


Figure 2: Controls on AMOC weakening at the end of the 21st century. Change in the AMOC strength for (a) SSP1-2.6, (b) SSP2-4.5, and (c) SSP5-8.5 emission scenarios. The scatter plots on the left show a comparison of the AMOC strength change predicted by the thermal-wind expression (x-axis) and the AMOC strength change in GCMs (y-axis). The proportion of variance accounted for and root-mean-square error are shown in the top left part of each panel. The bar plots on the right show the AMOC strength change predicted by Term A (white bar), Term B (hatched bar), and the higher-order residual terms (dotted bar) in the thermal-wind expression (Eq. 2). Term A represents changes in the Atlantic basin meridional density difference $\Delta_y \rho$, and Term B represents changes in the overturning depth H . The proportion of variance accounted for by each term is shown in the legend of each panel. The present-day time period is 1981–2010, and the SSP time period is 2070–2100. GCMs are ordered from weak to strong present-day AMOC.

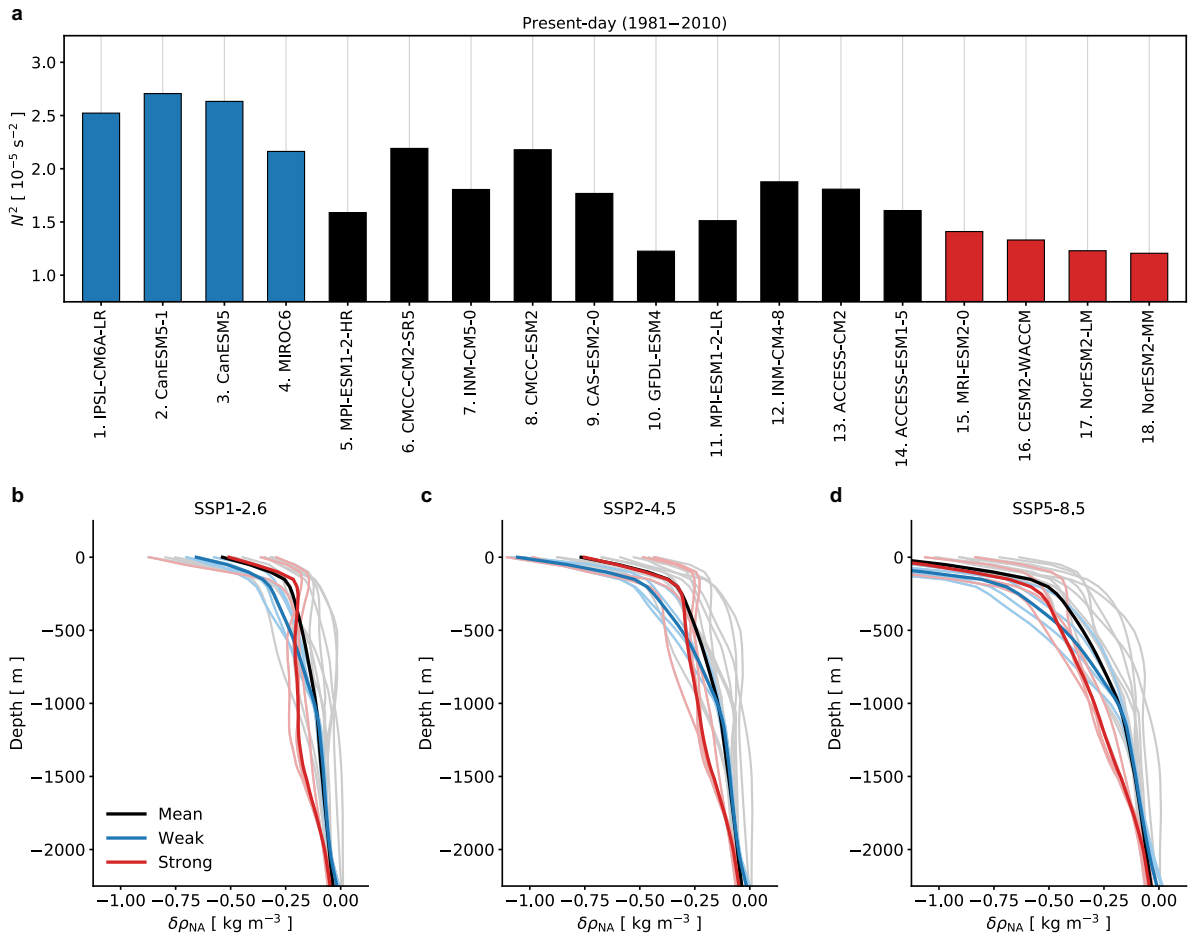


Figure 3: Relationship between present-day and future North Atlantic stratification. (a) The present-day stratification (N^2) of the North Atlantic (40°N – 65°N , 50 – 1000 m) from CMIP6 historical simulations. GCMs are ordered from weak to strong present-day AMOC. Change in the North Atlantic density ($\delta\rho_{NA}$) as a function of depth for (b) SSP1-2.6, (c) SSP2-4.5, and (d) SSP5-8.5 emission scenarios. The present-day time period is 1981–2010 and the SSP time period is 2071–2100. The thick lines denote the average of the four GCMs with the strongest present-day AMOC (red), the four GCMs with the weakest present-day AMOC (blue), and all other GCMs (black). Each thin line denotes an individual GCM.

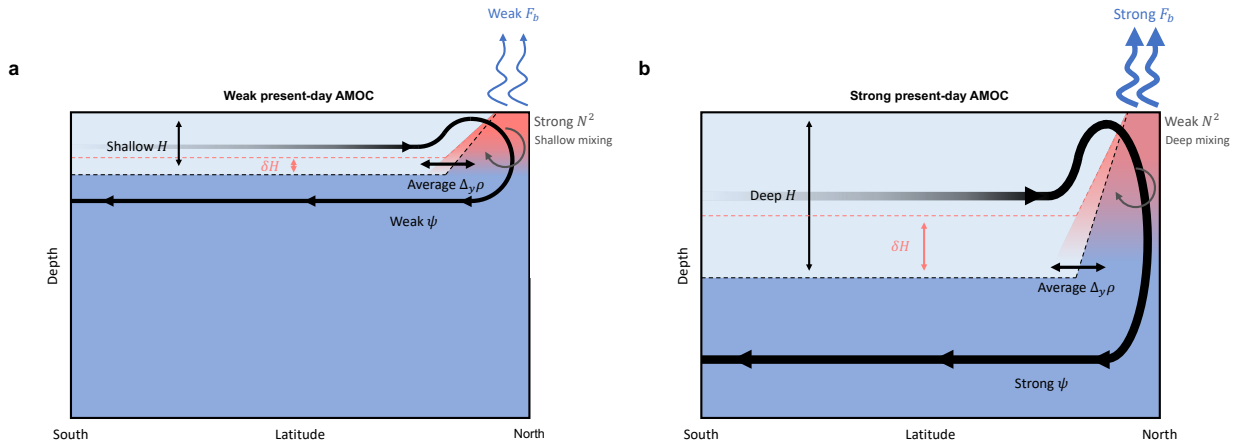


Figure 4: **Schematic depicting controls on the AMOC weakening under warming.** Processes that control the AMOC weakening under warming for GCMs with a (a) weak present-day AMOC and (b) strong present-day AMOC. The dashed line denotes the overturning depth (H). The streamline denotes the meridional overturning streamfunction or AMOC strength (ψ). The blue arrows denote surface buoyancy loss in the North Atlantic (F_b). The grey arrows denote the magnitude of North Atlantic stratification (N^2), which limits mixing deep into the Atlantic basin interior. The black double sided arrows and colors of each isopycnal layer denote the meridional density difference ($\Delta_y \rho$). GCMs with a deeper present-day H tend to have a stronger present-day AMOC and weaker present-day N^2 , which enables H to shoal more under warming (as indicated by the red dashed line), resulting in greater AMOC weakening. In other words, a stronger present-day AMOC and weaker present-day N^2 allows for deeper mixing of surface buoyancy flux anomalies into the North Atlantic water column (as indicated by the red shading) and results in greater shoaling and weakening of the AMOC through greater density changes at depth.

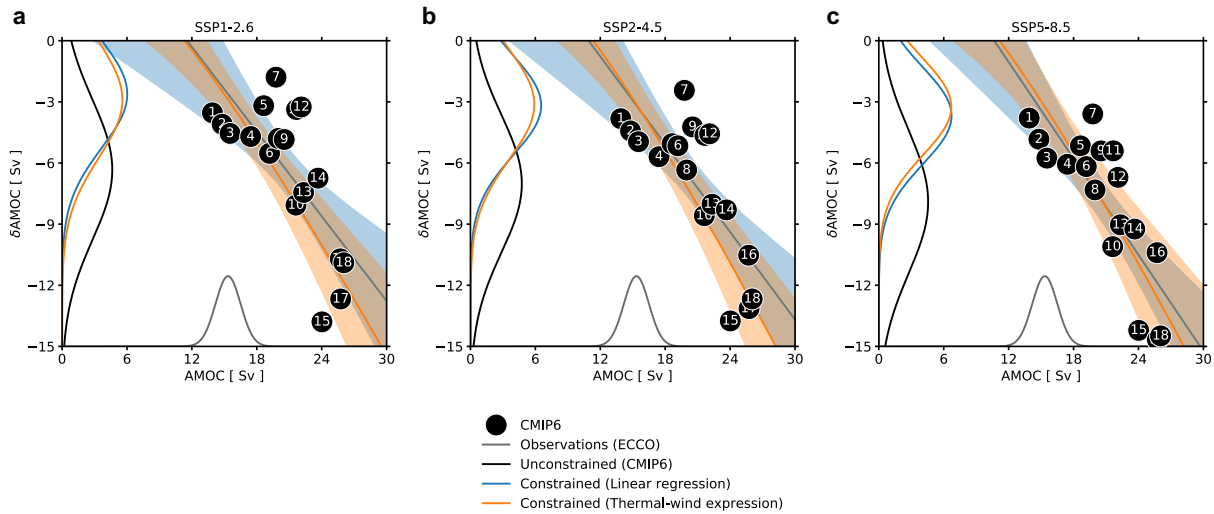


Figure 5: Constraints on AMOC weakening at the end of the 21st century. Scatter plot of the present-day (1981–2010) AMOC strength (x-axis) versus the change in AMOC strength (y-axis) under (a) SSP1-2.6, (b) SSP2-4.5, and (c) SSP5-8.5 emission scenarios for years 2071–2100. Each dot denotes a GCM (see Figure 1-3 for model number and model name). The blue line and shading in each panel denotes the linear regression and two standard deviations of the linear regressions, respectively. The orange line in each panel denotes Eq. (4), which predicts the AMOC strength change based on present-day H . The orange shading in each panel denotes the two standard deviations of the linear regressions between H and δH . The grey probability distributions denote observational estimates of the AMOC strength from ECCO. The black probability distributions denote the change in AMOC strength for years 2071–2100 using unconstrained CMIP6 GCMs. The blue probability distributions denote the change in AMOC strength for years 2071–2100 using CMIP6 GCMs constrained by Eq. (4) and observational estimates of the AMOC strength from ECCO. The orange probability distributions denote the change in AMOC strength for years 2071–2100 using CMIP6 GCMs constrained by Eq. (4) and observational estimates of the AMOC strength from ECCO.